JPn Neuroscience
The Journal of Physiology
J Physiol 594.22 (2016) pp 6607–6626

Cav1.2 and Cav1.3 L-type calcium channels independently control short- and long-term sensitization to pain

Houda Radwani[1,2,6], Maria José Lopez-Gonzalez[1,2], Daniel Cattaert[1,3], Olivier Roca-Lapirot[1,2], Eric Dobremez[1,4], Rabia Bouali-Benazzouz[1,2], Emelía Eiríksdóttir[5], Ülo Langel[5], Alexandre Favereaux[1,2], Mohammed Errami[6], Marc Landry[1,2,*] and Pascal Fossat[1,2,*]

[1] *University of Bordeaux, Bordeaux, France*
[2] *CNRS, IINS, UMR5297, Bordeaux, France*
[3] *CNRS, INCIA, UMR 5287, Talence, France*
[4] *Department of Pediatric Surgery, University Hospital of Bordeaux, Bordeaux, France*
[5] *Department of Neurochemistry and Neurotoxicology, Stockholm University, Stockholm, Sweden*
[6] *Faculty of Sciences, Abdelmalek Essaâdi University, Tetouan, Morocco*

Key points

- L-type calcium channels in the CNS exist as two subunit forming channels, Cav1.2 and Cav1.3, which are involved in short- and long-term plasticity.
- We demonstrate that Cav1.3 but not Cav1.2 is essential for wind-up.
- These results identify Cav1.3 as a key conductance responsible for short-term sensitization in physiological pain transmission.
- We confirm the role of Cav1.2 in a model of long-term plasticity associated with neuropathic pain.
- Up-regulation of Cav1.2 and down-regultation of Cav1.3 in neuropathic pain underlies the switch from physiology to pathology.
- Finally, the results of the present study reveal that therapeutic targeting molecular pathways involved in wind-up may be not relevant in the treatment of neuropathy.

Abstract Short-term central sensitization to pain temporarily increases the responsiveness of nociceptive pathways after peripheral injury. In dorsal horn neurons (DHNs), short-term sensitization can be monitored through the study of wind-up. Wind-up, a progressive increase in DHNs response following repetitive peripheral stimulations, depends on the post-synaptic L-type calcium channels. In the dorsal horn of the spinal cord, two L-type calcium channels are present, Cav1.2 and Cav1.3, each displaying specific kinetics and spatial distribution. In the present study, we used a mathematical model of DHNs in which we integrated the specific patterns of expression of each Cav subunits. This mathematical approach reveals that Cav1.3 is necessary for the onset of wind-up, whereas Cav1.2 is not and that synaptically triggered wind-up requires NMDA receptor activation. We then switched to a biological preparation in which we knocked down Cav subunits and confirmed the prominent role of Cav1.3 in both naive and spinal nerve ligation model of neuropathy (SNL). Interestingly, although a clear mechanical allodynia dependent on Cav1.2 expression was observed after SNL, the amplitude of wind-up was decreased. These results were confirmed with our model when adapting Cav1.3 conductance to the changes observed after SNL. Finally, our mathematical approach predicts that, although wind-up amplitude is decreased in SNL, plateau potentials are not altered, suggesting that plateau and wind-up are not fully equivalent. Wind-up and long-term hyperexcitability of DHNs are differentially controlled by

*These authors contributed equally to this work.

DOI: 10.1113/JP272725

Cav1.2 and Cav1.3, therefore confirming that short- and long-term sensitization are two different phenomena triggered by distinct mechanisms.

(Resubmitted 30 April 2016; accepted after revision 22 May 2016; first published online 27 May 2016)
Corrresponding author P. Fossat: CNRS UMR 5297, 146, rue leo saignat, 33077 Bordeaux Cedex, France. Email: pascal.fossat@u-bordeaux.fr

Abbreviations Cav1.2, L-channel comprising the α1c subunit; Cav1.3, L-channel comprising the α 1d subunit; DHNs, dorsal horn neurons; EMG, electromyographic; ICAN, non-specific calcium-activated channel; LTC, L-type calcium channels; MALDI-TOF, matrix-assisted laser desorption/ionization time-of-flight; MAP2, microtubule-associated protein 2; PD, post-discharge; PNA, peptide nucleic acids; SNL, spinal nerve ligation; VGCC, voltage-gated calcium channels; WDR, wide dynamic range.

Introduction

Dorsal horn neurons (DHNs) integrate sensory information and express an activity-dependent increase in responsiveness to nociceptive inputs termed central sensitization. Central sensitization is a physiological response to peripheral injury that lowers the pain threshold during tissue repair (Woolf 1991; Basbaum *et al.* 2009). However, central sensitization can be maintained for days even if the primary cause of pain has disappeared, thus resulting in a switch from physiology to pathology. For example, chronic neuropathic pain induced by nerve lesions, as in the spinal nerve ligation model (SNL), is associated with abnormal allodynia that is pathologically maintained beyond tissue repair. Physiological central sensitization can be assessed by repetitive nociceptive stimulations at low frequency presenting as a wind-up of DHNs. A crucial question in understanding the neuropathic pain mechanisms is whether the wind-up, as a short-term sensitization process, is involved in the SNL-induced hyperexcitability. However, this question has never been clearly assessed. The wind-up is sustained by voltage-gated calcium channels (VGCC) of the L-type (LTC) (Morisset and Nagy 2000; Fossat *et al.* 2007). LTC can also control plateau potentials, which comprise a mechanism of input/output amplification allowing the development of the wind-up (Morisset and Nagy 1999; Morisset and Nagy 2000). Of the four different LTC subunits, only Cav1.2 and Cav1.3 are expressed in the dorsal horn of the spinal cord. Cav1.3 subunits have kinetics close to low voltage-activated calcium channels of the Cav3.x family, whereas Cav1.2 are high-voltage activated (Xu and Lipscombe 2001; Helton *et al.* 2005). Cav1.3 are localized in dendritic compartments, whereas Cav1.2 are preferentially restricted to the soma (Simon *et al.* 2003; Dobremez *et al.* 2005). These differences suggest that Cav1.2 and Cav1.3 play different roles in DHN physiology and thus in plateau potentials and wind-up. Moreover, Cav1.2 and Cav1.3 are regulated oppositely in neuropathic rats (Fossat *et al.* 2010; Favereaux *et al.* 2011). However, whether Cav1.2 or Cav1.3 controls the wind-up is not known. This information could answer the question regarding the potential implication of the wind-up in the SNL-induced hyperexcitability of DHN. Indeed, if wind-up is involved, it should be controlled by the up-regulated Cav1.2 that also controlled SNL-induced hyperexcitability of DHN. In the present study, we assessed this question by combining a computational model of DHNs in which we manipulated Cav1.2 and Cav1.3 conductances with *in vivo* experiments in which we down-regulated the expression of Cav1.2 and Cav1.3 mRNA, in both normal and SNL-induced allodynia conditions. In the mathematical model, we set DHNs parameters in accordance with those recorded in spinal slices (Derjean 2002) and we distinguished Cav1.3 and Cav1.2 conductances according to their specific kinetic and spatial distribution (Xu and Lipscombe 2001; Simon *et al.* 2003; Dobremez *et al.* 2005; Helton *et al.* 2005). Then, we recorded the wind-up of a nociceptive flexion reflex in anaesthetized rats together with an anti-sense strategy to block the expression of each LTC subunit. In both computational model and *in vivo* experiments, we found that the wind-up was under the exclusive control of Cav1.3, suggesting that wind-up and long-term hyperexcitability were dissociated. In support of these results, we found that the wind-up was decreased in SNL conditions, consistently with the decrease of Cav1.3 expression in this model. Taken together, our data indicate that Cav1.3 controls the onset of wind-up, and that DHN hyperexcitability and subsequent pathological changes are independently under the control of Cav1.2.

Methods

All experimental procedures followed the ethical guidelines of the International Association for the Study of Pain (IASP) and were approved by the local ethic committee (agreement no. 330110005-A).

Immunohistochemistry

Control, sham, SNL and anti-sense-injected rats were perfusion-fixed through the ascending aorta with 4% paraformaldehyde in phosphate buffer (0.1 M,

pH 7.4). Double immunodetection of Cav1.2 or Cav1.3 and microtubule-associated protein 2 (MAP2), a somatodendritic neuronal marker, was performed on spinal cord cryostat sections (30 μm thickness; Microm, Bicester, UK). Briefly, sections were incubated overnight at 4°C with mouse anti-MAP2 (dilution 1:1000; Sigma, St Louis, MO, USA) and rabbit anti-Cav1.2 or anti-Cav1.3 (dilution 1:200; Alomone, Jerusalem, Israel) antibodies. After rinsing, the sections were incubated with biotinylated goat anti-rabbit antibody (dilution 1:200; Vector Laboratories, Burlingame, CA, USA) and next with Alexa 488-conjugated streptavidin (dilution 1:500) and Alexa 568-conjugated goat anti-mouse (dilution 1:500) antibodies (Molecular Probes/Invitrogen, Carlsbad, CA, USA). The sections were then mounted and viewed with a confocal microscope (Leica SP2; Leica Microsystems, Wetzlar, Germany). Specificity of antibodies was determined as described previously (Dobremez *et al.* 2005). Immunohistochemistry after anti-sense strategy was performed after intrathecal injection of either anti-Cav1.2, anti-Cav1.3 or mismatch peptide nucleic acids (PNA, see below).

For immunofluorescence quantification, Cav1.2- and Cav1.3-immunolabelled sections were viewed with a confocal microscope (Leica SP2; Leica Microsystems). Images to be compared were collected during the same session using identical scanning settings. They were then imported into ImageJ, version 1.42q (NIH, Bethesda, MD, USA) for quantitative analysis. Background was subtracted by thresholding and the mean grey level corresponding to fluorescence intensity was measured.

Mathematical model of DHNs

The model neuron (recorded at 36°C) was implemented using the simulation software Neuron, version 7.3 (http://www.neuron.yale.edu) in accordance with a previous model (Aguiar *et al.* 2010). It was composed of a cell body (diameter 20 μm), a dendrite (length 500 μm, diameter 4 μm), an axon hillock (decreased in diameter from 2 to 1 μm along a length of 3 μm) and an axon (length 1000 μm, diameter 1 μm). All compartments were equipped with ionic channels in accordance with the description given by Aguiar *et al.* (2010), except for the iCaL, which was replaced by Cav12 and Cav13. For the *I*/*V* properties, see Xu and Lipscombe (2001).

For Cav12, tau_m and m_inf where:

$$\begin{aligned} \text{tau\_m} &= 1/(a + b)/\text{tadj} \\ \text{m\_inf} &= 1/(1 + \exp[(v + 39.4)/-7]) \\ a &= 1.6/(1 + \exp[-0.072 \times (v + 16)]) \\ b &= 0.02 \times \text{vtrap}[-(v + 39.4), 5.36] \end{aligned}$$

Table 1. Conductance distribution in WDR neurons

	Soma	Axon	Dendrite
gNaHH	0.04	0.04	0
gKHH	0.05	0.05	0
gCAV13	3.5 e-06	0	3.5×10^{-6}
gCAV12	1.4 e-05	0	0
gCAN	0	0	0.00007
gKCa	0.0001	0	0.001
gNaP	0.0001	0	0
giA	0	0	0
gPas	0.000042	0.000042	0.000042

g in S.cm^{-2}.

For Cav13, tau_m and m_inf where:

$$\begin{aligned} \text{tau\_m} &= 1/(a + b)/\text{tadj} \\ \text{m\_inf} &= 1/(1 + \exp[(\text{v} + 39.4)/-7]) \\ a &= 1.6/(1 + \exp[-0.072 \times (\text{v} + 16)]) \\ b &= 0.02 \times \text{vtrap}[-(\text{v} + 39.4), 5.36] \end{aligned}$$

Calcium dynamics in neurons was simulated as described in Aguiar *et al.* (2010). The internal calcium concentration resulted from calcium currents and a pump:

$$\begin{aligned} \text{drive\_channel} &= -(10\,000) \times \text{ica}/(2 \times \text{FARADAY} \times \text{depth}) \\ \text{with depth} &= 0.1\ \mu\text{m} \\ \text{cai\_new}' &= \text{drive\_channel} + (\text{cai\_inf-cai\_new})/\text{cai\_tau} \\ \text{cai} &= \text{cai\_new} \\ \text{with cai\_tau} &= 2\ \text{ms and cai\_inf} = 50 \times 10^{-6}\ \text{mM} \end{aligned}$$

The properties of the various ion channels used in the simulations are based on Hodgkin–Huxley formalism (a detailed description of these equations is given in Aguiar *et al.* (2010). The density of each channel type (Table 1) was adjusted to fit the experimental results. The connection from C-fibres was mediated by a relay interneuron with the same morphological features as the wide dynamic range (WDR) neuron. Channel equipment of the relay interneuron was set as described in Aguiar *et al.* (2010). Finally, the parameters used for each type of synapse, in each type of connection, are summarized in Table 2. We also added stochastic synaptic noise with excitatory and inhibitory inputs to make the model more realistic and allow a statistical approach. The integration time step was set to 0.0125 ms and three repetitions were performed for each experimental condition.

Table 2. Synaptic inputs

Synaptic inputs	Conductance
gAMPA C fibre to interneuron	0.008
gNMDA C fibre to interneuron	0.004
gNK1 C fibre to interneuron	0.00002
gAMPA interneuron to WDR	0.0002
gNMDA interneuron to WDR	0.0002
gNK1 interneuron to WDR	0.000015
gGABA interneuron to WDR	0.0002
gExcitatory synaptic noise	0.001
gInhibitory synaptic noise	0.001

g in $S.cm^{-2}$.

Animals

We used male wistar rats aged >21 postnatal days, weighing 55–350 g. All rats presenting locomotor deficiency or a significant decrease of weight were not included. Rats were killed by an overdose of anaesthetic (urethane) and dorsal lumbar tissues were kept at –80°C for quantitative RT-PCR (see below).

Anaesthesia

Surgery was performed under gaseous anaesthesia with isoflurane 5 % for induction and 2 % for maintenance. Electrophysiological recordings were performed with an I.P. injection of urethane 1.5 g kg^{-1}.

Drug application

Nicardipine hydrochloride (Sigma) was dissolved in distillated water for a stock solution of 10 mM. A solution of 100 μM prepared in saline (NaCl 0.9 %) from the stock solution was superfused above the spinal cord during nociceptive flexion reflex recordings.

PNA design and application

PNA sequences (15 mers) were designed to target regions immediately upstream of the translation start site of Cav1.2 and Cav1.3 mRNA. Care was taken to minimize the stability of hairpin secondary structures in physiological conditions:

Anti-Cav1.2 PNA: Cys-CGTGAGATTGTAATG
Anti-Cav1.3 PNA: Cys-GTTACTGATAGGTAG
Mismatch PNA: Cys-CGTGAATTAGTTAGG

To improve their intracellular delivery, cysteine-extended PNA were coupled to the cell-penetrating peptide transportan TP10 (AGYLLGKINLKALAALA KKIL-amide) (Soomets *et al.* 2000) via a disulphide bond. After reduction of the bond in the intracellular medium, transportan-PNA constructs were dissociated and PNA could either associate with target Cav1.2 or Cav1.3 mRNA in the cytosol or translocate into the nucleus, thereby interacting with the corresponding DNA sequences.

PNA were synthesized automatically on an 433A peptide synthesizer (Applied Biosystems, Foster City, CA, USA) using the *t*-Boc strategy (Egholm *et al.* 1993; Koch *et al.* 1997). The carrier peptide, transportan (TP10), was synthesized on the 431A peptide synthesizer and purified before conjugation with PNA on a reverse-phase HPLC C_{18} column. The masses of the purified peptide and PNA were verified by matrix-assisted laser desorption/ionization time-of-flight (MALDI-TOF) (ABI Voyager-DE STR; Applied Biosystems) mass spectrometry. Conjugation was performed in DMSO/dimethylformamide/0.1 M acetic buffer (pH 5.5) (1:1:3 mixture overnight) and the products were separated on a C_{18} HPLC column. A detailed description of the conjugation is provided in Pooga *et al.* (2002). The correct conjugate was determined by absorbance profile in multiwavelength detector of the HPLC and by MALDI-TOF mass spectrometry. Transportan-PNA constructs were injected daily for 4 days, which is a time-interval consistent with calcium channel turn-over (Lambert *et al.* 1998; Dobremez *et al.* 2005).

In vivo electromyographic (EMG) recordings

An EMG study was carried out on male rats in the weight ranges 250–350 g and 55–60 g. Rats were placed in a stereotaxic frame to ensure stability during electrophysiological recordings. Recordings were made in the ipsilateral biceps femoris muscle with two teflon-coated stainless steel electrodes (diameter 200 lm; Phymep, Paris, France). Electrical stimuli (1 ms, single shocks, master 8 stimulator; AMPI, Jerusalem, Israel) were delivered with electrodes placed under the paw skin in the region of the sural nerve. A maximum response was obtained for a stimulus intensity of 60–80 V, as determined with single shocks delivered at 30 s intervals to avoid central sensitization. At this stimulus intensity, a slight muscle contraction was elicited without movement of the limb.

Quantitative RT-PCR

Total RNA was purified with the QIAzol lysis Reagent (Qiagen, Valencia, CA, USA) in accordance with the manufacturer's instructions. cDNA was synthesized using Maxima First Strand cDNA Synthesis Kit (Thermo Scientific, Waltham, MA, USA). PCR amplification was performed on a LightCycler LC480 (Roche, Basel, Switzerland) with primer pairs designed to span exon boundaries and to generate amplicons of ~100 bp. Primer sets for Sdha, Cacna1c and Cacna1d were tested by quantitative RT-PCR and gel electrophoresis for the absence of primer–dimer artefacts and multiple

products. cDNA dilution curves were performed to assess primer efficiency and linearity over a large range of cDNA concentrations. Triplicate quantitative RT-PCR reactions were performed twice for each sample, using transcript-specific primers (600 nM) and cDNA (10 ng) in a final volume of 10 μl. The SYBR Premix Ex Taq II (Takara) was used in accordance with the manufacturer's instructions. The Ct value of each gene was normalized against that of Sdha. The relative level of expression was calculated using the comparative ($2^{-\Delta\Delta Ct}$) method (Livak and Schmittgen, 2001).

Quantitative RT-PCR primers:

Sdha, Fw: 5′-TGCGGAAGCACGGAAGGAGT-3′
Sdha Bw: 5′-CTTCTGCTGGCCCTCGATGG-3′
Cacna1c Fw: 5′-AAGCAAGAACAAACCACTG-3′
Cacna1c Bw: 5′-TGACACAACTCACAATCGT-3′
Cacna1d Fw: 5′-CCTCAACCATCGGTCTAGCA-3′
Cacna1d Bw: 5′-GCACAGAAACCAGGAACCAG-3′

Behavioural tests

Rats were placed in the testing cage 1 h before the test for habituation. The limb withdrawal threshold was measured with an electronic device (Bioseb, Vitrolles, France). A progressive pressure is applied, with pipette tip connected to a force sensor, under the paw of the hindlimb until the animals withdraw the limb, and the pressure value (g) is collected. This procedure is repeated three times separated by 1 min to obtain an average value. Mechanical response thresholds were monitored before surgery, and at days 7 and 11 (24 h after the last PNA injection) after surgery.

Surgical procedures

We used the same experimental procedure as that described by Fossat *et al.* (2010). A catheter (PE-10; Phymep) was inserted into the subarachnoid space and the tip was pushed into the L5 region. The external portion of the catheter was placed under the skin up to the neck. The incision was closed using 3-0 surgical sutures. For anti-sense injections, rats were first subjected to gaseous anaesthesia with halothane (5% for induction and 2% for maintenance). Anti-sense was injected using a Hamilton syringe connected to the catheter and flushed with 10 μl of saline (dead volume of the catheter). Experiments were performed 24 h after the last injection. To determine whether the PNA injection was performed in the area of interest (lumbar part of the spinal cord), a volume of 10 μl of xylocaine was injected. This dose elicits a reversal paralysis of the animal hindlimb with a complete recuperation within a few minutes. All rats with no paralysis were rejected.

For the SNL procedure, we used a surgical procedure derived from (Kim and Chung, 1992). The right L5 spinal nerve was isolated and tightly ligated with a 7.0 silk thread. After complete haemostasis, the incision was sutured. Surgery was performed on all rats under gaseous anaesthesia with a mixture of isoflurane (5% for induction and 2% for maintenance) and a 1:1 flow ratio of air/O_2.The rats resumed normal activity within 30 min after termination of the gaseous anaesthesia.

In vivo extracellular recordings

A laminectomy was performed on lumbar vertebrae L1–L3 and segments L4–L5 of the spinal cord were exposed. Extracellular recordings of WDR DHNs were made with borosilicate glass capillaries (2 MΩ, filled with NaCl 684 mM) (Harvard Apparatus, Cambridge, MA, USA). Electrodes were descended with a micro-drive (Unimécanique, Asnières, France). The depth of the neurons from the surface of the dorsal horn of the spinal cord was monitored. This depth was comparable in all groups tested (652 ± 83 to 762 ± 43 μm). The criterion for the selection of a neuron was the presence of a Aβ-fibre-evoked response followed by a C fibre-evoked response to electrical stimulation of the ipsilateral paw.

Wind-up protocol

For EMG recordings, we recorded myographic responses following transcutaneous electrical stimulation of the centre of the receptive field. A sequence of 15 stimuli was delivered at 1 Hz. Each stimulus was a single shock at ~80% of the intensity eliciting a maximal response. Each sequence of 15 stimuli was separated by at least 5 min to avoid cumulative effects. We used Spike 2 software (Cambridge Electronic Design, Cambridge, UK) to detect myographic units and we calculated the number of spikes following each electric shock with a delay of 80 ms. For extracellular recordings, responses were elicited by a train of 15 transcutaneous stimuli (1 Hz frequency) over the threshold for C fibres. The Aβ, Aδ and C fibre evoked responses were taken as the action potentials within a time frame of 0–20, 20–90 and 90–300 ms respectively (Suzuki *et al.* 2001). The remaining neuronal response (300 ms to 1 s post-stimulus) was taken as the post-discharge (PD) of the neuron. We focused on the C+PD part of the response. We calculated a wind-up coefficient by measuring the difference between the sum of C+PD responses in all 15 stimuli and the baseline response (i.e. fifteen times the number of action potentials of the first response). Electrophysiological data were acquired using a CED 1401 interface and analysed with Spike 2 software (Cambridge Electronic Design). Data were plotted using Prism (GraphPad Software Inc., San Diego, CA, USA). All values are reported as the mean ± SEM (with n indicating the number of animals in the EMG recordings or number of WDR in extracellular

recordings). Wind-up plots were normalized to the first response of the series. Statistical analysis was conducted using Prism software. For electrophysiological recordings, we compared all experimental conditions by a statistical comparison of the wind-up coefficient. $P < 0.05$ was considered statistically significant.

Results

Cav1.3 is essential for wind-up in a computational model of DHNs

We used a mathematical model of DHNs to simulate the respective role of each LTCs in plateau potential and wind-up. In this mathematical model, we used published Cav1.2 and Cav1.3 kinetics (Xu and Lipscombe, 2001; Helton *et al.* 2005). We placed Cav1.3 in the soma and dendrites (Table 1) and restricted Cav1.2 to the somatic compartment in line with the immunohistochemical data (Fig. 1*A*) (Dobremez *et al.* 2005). Indeed, Cav1.2 is restricted to the soma, whereas Cav1.3 is localized in soma and dendrites. We performed a quantitative RT-PCR of Cav1.2/Cav1.3 mRNA in the dorsal part of the lumbar spinal cord to obtain an approximation of the proportion of each Cav subunit and to set the corresponding current in the computational model. The Cav1.2 expression level is two-fold higher than Cav1.3 (Cav1.3 was 44 ± 1.6 % of Cav1.2, $P < 0{,}001$, Wilcoxon signed rank test, $n =$ 17 rats). We analysed the capacity of DHNs to generate plateau potentials in the presence or absence of each LTC current. In the absence of LTCs, a large square current pulse (2 s) did not generate plateau but, instead, tonic discharge (Fig. 1*B1*). Repetitive short square current pulses induced a constant discharge frequency (Fig. 1*B2*). When both LTCs were added, the same large current pulse induced a plateau potential followed by PD (Fig. 1*C1*). Repetitive short current pulses triggered a wind-up of DHN discharge (Fig. 1*C2*). The wind-up coefficient was significantly different between both conditions (−7 ± 4 Cav1.3–/Cav1.2– *vs.* 98 ± 2 Cav1.3+/Cav1.2+, $n = 6$, $P < 0.01$, Mann–Whitney test) (Fig. 1*D* and *E*). We next analysed the role of each sub-unit in the expression of plateau potentials and wind-up. When Cav1.3 was expressed alone, plateau potentials and wind-up were expressed (Fig. 2*A1* and *A2*). The lower Cav1.3 conductance necessary for appearance of plateau was 10^{-6} S cm^{-2} and the maximum amplitude was reached for 10^{-5} S cm^{-2} at 40pA (intensity of stimulation) (Fig. 2*A3*). By contrast, when Cav1.2 was expressed alone, DHNs exhibited a constant discharge frequency with no PD and no wind-up was expressed (Fig. 2*B1* and *B2*). Plateau was not elicited, regardless of the intensity of stimulation (Fig. 2*B3*). We calculated a wind-up coefficient for Cav1.3 or Cav1.2 alone and we observed a significant difference between both conditions (94 ± 1 Cav1.3+/Cav1.2– *vs.* –3 ± 8 Cav1.3–/Cav1.2+, $n = 6$, $P < 0.01$, Mann–Whitney test) (Fig. 2*C* and *D*). Therefore, simulations predict that Cav1.3 but not Cav1.2 is essential for the expression of plateau and wind-up.

Next, we added a synaptic component to the DHN model and evaluated the role of Cav1.2 and Cav1.3 in the wind-up of DHNs following stimulation of afferent C-fibres. C-fibres are connected to the DHNs through interneurons containing AMPA, NMDA and NK1 excitatory receptors. When both LTCs subunits are present, repetitive stimulations of C-fibres at 1 Hz induced a wind-up of DHNs (Cav1.2+/Cav1.3+; wind-up coefficient 137 ± 1, $n = 6$) (Fig. 3*A*, *D1* and *D2*). Wind-up is still expressed when Cav1.2 is removed (Cav1.2–/Cav1.3+; wind-up coefficient 71 ± 12, $n = 6$) (Fig. 3*B*, *E1* and *E2*). By contrast, with no Cav1.3, only very slight wind-up is observed (Cav1.2+/Cav1.3–; wind-up coefficient 14 ± 1, $n = 6$) (Fig. 3*C* and *D*), mainly as a result of NMDA receptor activation during C-fibre stimulations (Fig. 4). This result confirms the role of Cav1.3 in setting the amplitude of wind-up, and the need for a synaptic component (e.g NMDA receptor) for the onset of wind-up. By contrast, Cav1.2 has no role in wind-up in this model. To test the physiological relevance of these results, we used a biological preparation to analyse the impact on wind-up of the blockade of Cav1.2 and Cav1.3.

LTCs control the onset of wind-up in young and adult rats

Classically, *in vitro* studies on the wind-up of DHNs are performed on spinal slices from 3-week-old rats, whereas *in vivo* studies are generally made on 2–3-month-old rats (Thompson *et al.* 1990; Kim and Chung, 1992; Morisset and Nagy, 1998; Derjean *et al.* 2003). We first compared the wind-up of the nociceptive flexion reflex in these two age groups aiming to identify a possible difference in amplitude or molecular mechanisms (Fig. 5). A stable nociceptive reflex was obtained by electrical stimulations of high threshold afferents in the sural nerve region of the paw. When the stimulus was repeated at low frequency (1 Hz), the reflex magnitude gradually increased during the sequence of stimulation, featuring the wind-up of the flexion reflex (Gozariu *et al.* 1997). The number of muscular units activated increased across the 15 shocks (Fig. 5*A* and *B*). Wind-up is similar in amplitude between the two age groups (wind-up coefficient was 517 ± 148.7, in 250–300 g rats and 511 ± 104.7 in 55–60 g rats, $n = 15$, $P = 0.67$, Mann–Whitney test) (Fig. 5*E1* and *E2*) and is sensitive to the LTC blocker nicardipine in the two group of rats (for 250–300 g rats, the wind-up coefficient decreased from 397 ± 126 in control to 48 ± 15.2, $n = 7$, $P < 0.05$, Wilcoxon matched-pair ranked; for 55–60 g rats, the wind-up coefficient decreased from 534 ± 126.6 in control to 54 ± 34.8, $n = 7$, $P < 0.05$, Wilcoxon

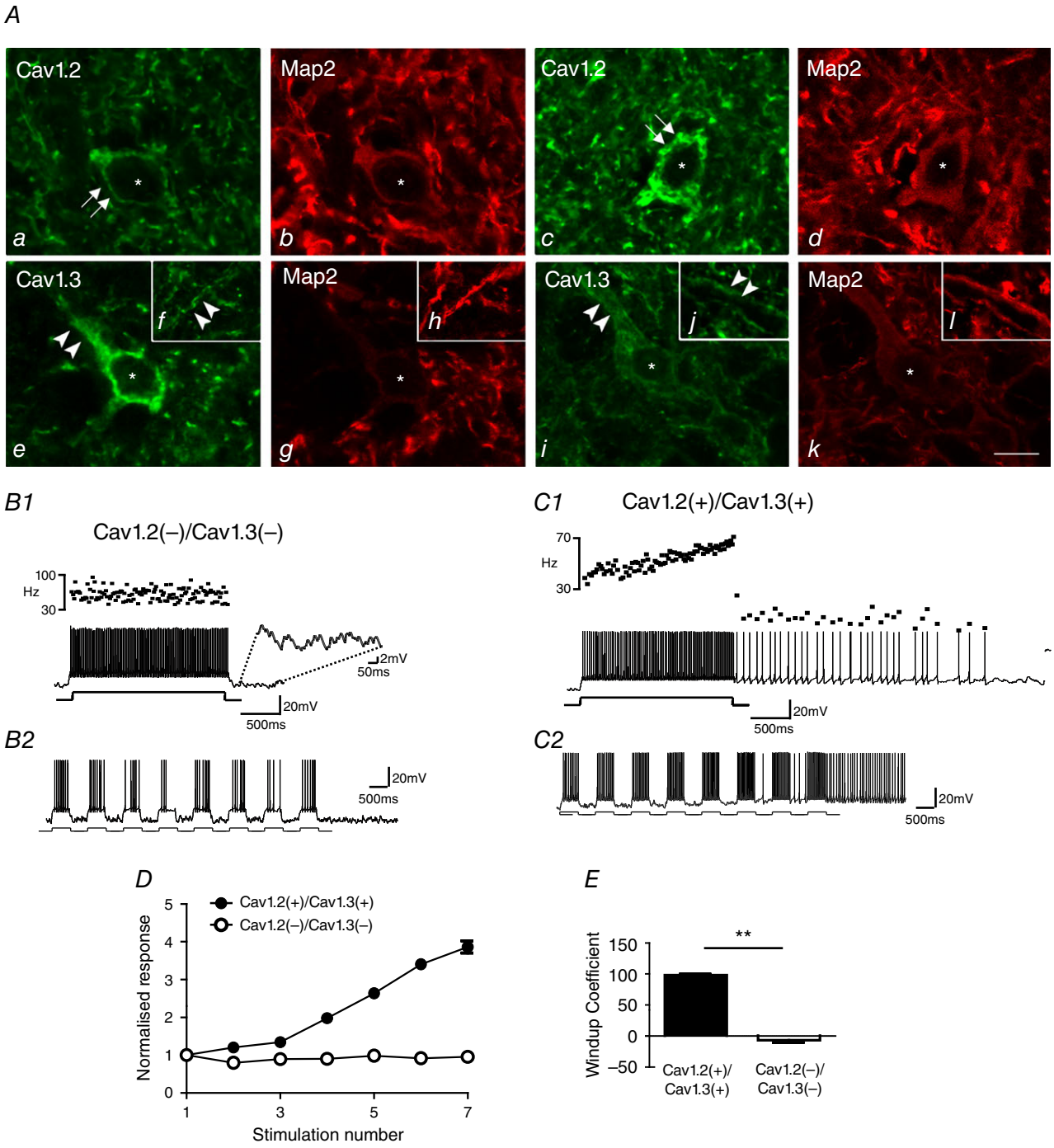

Figure 1. Computational model of DHN discharge pattern with or without LTCs
A, Cav1.2 (*a* and *c*) and Cav1.3 (*e* and *i*) are expressed in different subcellular compartments of deep dorsal horn neurons (white stars) as shown with Map2 co-detection (*b*, *d*, *g* and *k*). Cav1.2 labelling is restricted to the soma (double arrows in *a* and *c*). Cav1.3 is found in the cell body but also in proximal (double arrowheads in *e* and *i*) and more distal dendrites [double arrowheads in *e* and *i* inset (labelled *f* and *j*)]. No changes in localization are observed after nerve injury (SNL, *c* and *i* and inset labelled *j*) compared to control conditions (Sham, *a* and *e* and inset labelled *f*). Scale bar = 10 μm. *B1* and *B2*, DHN discharge pattern without LTCs. *B1*, DHNs response to application of a square current pulse (2 s). Note that DHN presents a tonic response with a constant discharge frequency. *B2*, DHN response to a series of eight short (500 ms) square current pulses. Response of DHN was the same for all current pulses. *C1* and *C2*, DHN discharge pattern with LTCs. In response to a square current pulses (2 s), DHN discharge frequency progressively increased showing a plateau potential, followed by PD (C1). Repetitive square current pulses (500 ms × 8) induced a progressive increase in the DHN response followed by PD revealing a wind-up of DHN discharge (C2). *D*, normalized response. *E*, wind-up coefficient.

matched-pair ranked) (Fig. 5*F* and *G*). Because wind-up is similar in two age groups, subsequent experiments were conducted in the two age groups. Experiments in naive rats were performed in young rats (55–60 g) and SNL experiments were performed in older rats (250–350 g).

Knockdown of LTC channels

We next tested the involvement of the LTC subunit in wind-up in both naive rats and rats with spinal nerve ligation. To suppress the expression of LTCs, we used an anti-sense strategy. We injected intrathecally anti-Cav1.2, anti-Cav 1.3 or mismatch PNA daily for 4 days based on

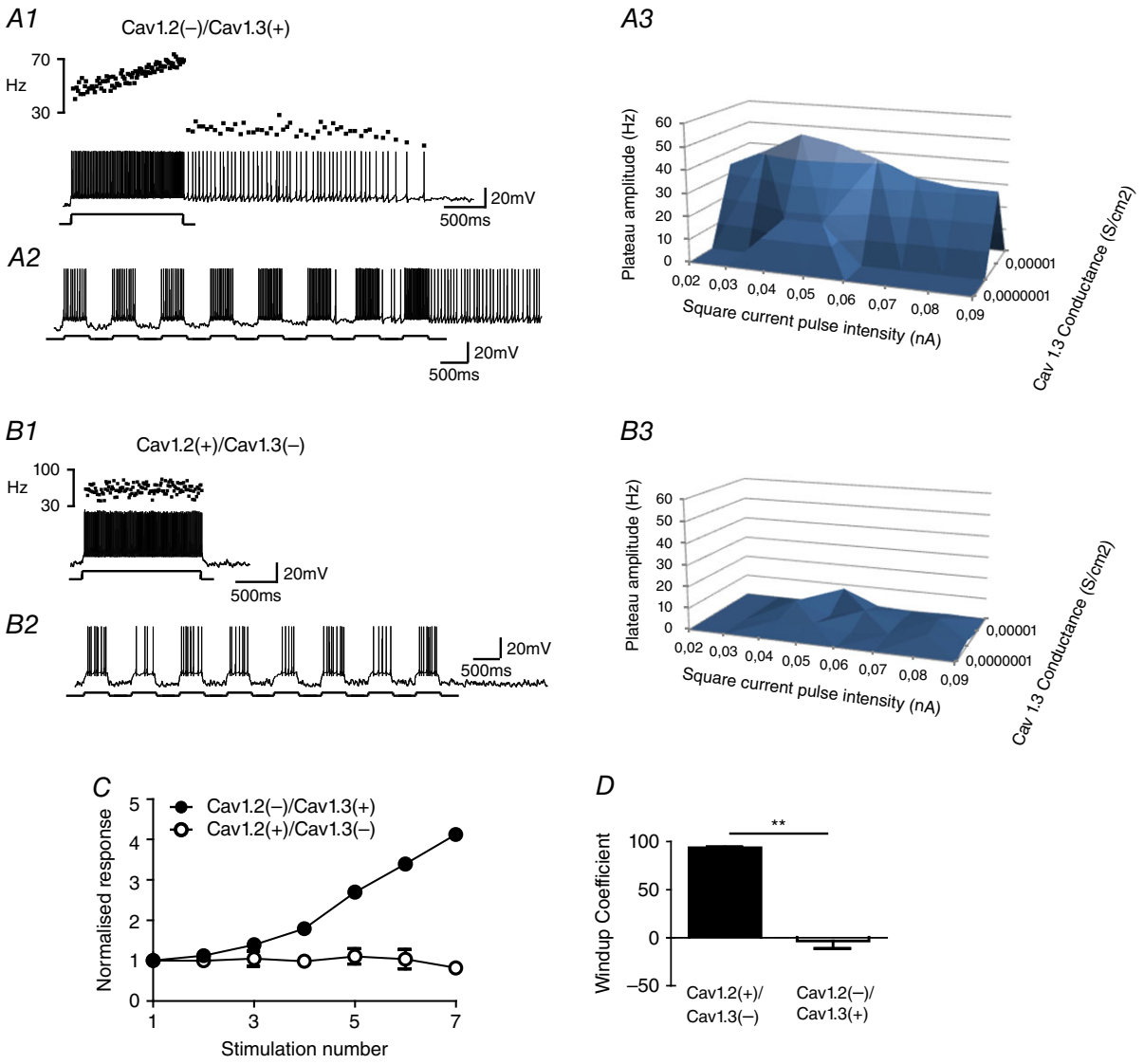

Figure 2. Role of Cav1.2 and Cav1.3 on plateau potentials and wind-up in a computational model of DHNs
A1 and *A2*, DHN discharge pattern after Cav1.2 removal. With Cav1.3, DHNs exhibit plateau potential (*A1*) and wind-up (*A2*). *A3*, amplitude of plateau potentials according to the amplitude of the Cav1.3 conductance and the amplitude of the stimulation (amplitude of plateau is measured as the difference in discharge frequency at the end of the stimulus *vs*. discharge frequency at the beginning of the stimulus). Plateau appears at low stimulus intensity (40 pA) and low conductance (0.5 μS cm^{-2}). A peak of plateau amplitude is reached for a stimulation intensity of 40 pA and a conductance of 10 μS cm^{-2}. A PD appeared at 5 μS cm^{-2} for a stimulation intensity of 30 pA. *B1* and *B2*, DHN discharge pattern after Cav1.3 removal. Cav1.3 removal converts a plateau DHN into a tonic DHN (*B1*). No wind-up is observed (*B2*). *B3*, in the absence of Cav1.3 in dendrites, neither plateau potentials, nor wind-up was observed, regardless the intensity of stimulation. *C*, normalized response. Wind-up is still present when Cav 1.3 subunit is present alone but is suppressed when Cav 1.2 is removed. *D*, wind-up coefficient. [Colour figure can be viewed at wileyonlinelibrary.com]

the reported turn-over of LTCs (Dobremez *et al.* 2005). We evaluated the efficiency of these anti-sense molecules both at the transcript, as well as at the protein level (Fig. 6). Injection of the anti-sense daily for 4 days significantly reduced the corresponding mRNA (Fig. 6*A*) [ANOVA ($P < 0.001$) followed by Bonferroni's multiple comparison test, Cav1.2 expression was 19 ± 5% of control with anti-Cav1.2 PNA injection, $P < 0.01$, and 102 ± 18% of control with mismatch PNA, $P > 0.05$, $n = 6$ in each group (control, Anti-Cav1.2 and mismatch); ANOVA ($P < 0.01$) followed by Bonferroni's multiple comparison test, Cav1.3 expression was 22.5 ± 7.4% of control with anti-Cav1.3 PNA injection, $P < 0.05$, and 112 ± 25% of control with mismatch PNA, $P > 0.05$, $n = 7$ for control, $n = 4$ for Anti-Cav1.3 and $n = 5$ for mismatch). We next investigated knockdown at the protein level by immunostaining for Cav after PNA treatment (Fig. 6*B–D*). We observed that Cav immunoreactivity is decreased by the corresponding anti-sense molecule but not the unrelevant PNA (Fig. 6*B*). The intensity of the immunolabelling for Cav1.2 was significantly reduced when Anti-Cav1.2 was injected but not with the mismatch molecule (Fig. 6*C*) [ANOVA ($P < 0.001$) followed by Bonferroni's multiple comparison test, 57.4 ± 9.4% of Sham, $P < 0.01$]. Again, the intensity of immunolabelling was significantly reduced when Anti-Cav1.3 was injected but not with the mismatch molecule (Fig. 6*D*) [ANOVA ($P < 0.001$) followed by Bonferroni's multiple comparison test, 53 ± 13.7% of Sham, $P < 0.001$]. The knockdown induces a 50% decrease in the protein level that is sufficient to induce a biological effect (Fossat *et al.* 2010), maybe as a result of a threshold effect where the level of protein reached is too low to be efficient.

Cav1.3 mediates the onset of wind-up *in vivo*

We first analysed the consequence of LTC knockdown on the wind-up of a nociceptive flexion reflex (Fig. 7). Wind-up amplitude was similar between 'mismatch' PNA and sham animals (Fig. 7*A1* and *A2*) (wind-up coefficient was 723 ± 142, $n = 8$, for mismatch and 510 ± 90, $n = 13$, for Sham, $P = 0.14$, Mann–Whitney test) (Fig. 4*B1* and *B2*). The amplitude of wind-up was no different between sham and animals treated with anti-Cav1.2 PNA (Fig. 7*A3*) (wind-up coefficient was 510 ± 90, $n = 13$ for Sham and 377 ± 110, $n = 8$ for anti-Cav1.2, $P = 0.49$,

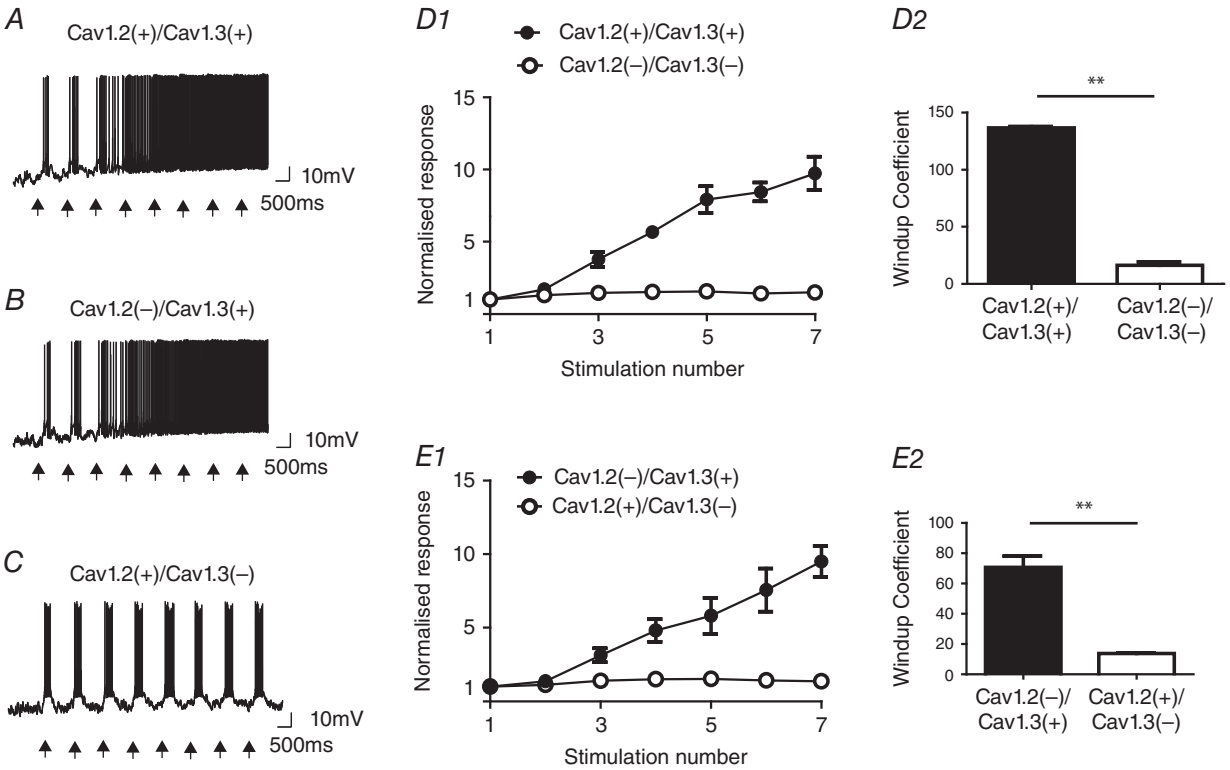

Figure 3. Computational model of DHNs response to repetitive C-fibre stimulations
A1, DHNs with LTCs (Cav1.2+/Cav1.3+) respond to repetitive C-fibre stimulations by a progressive increase in the number of spikes followed by PD revealing wind-up (arrows indicate C-fibre stimulations). *B*, Cav1.2 (Cav1.2–/Cav1.3+) removal does not suppress the wind-up induced by repetitive C-fibre stimulations. *C*, Cav1.3 removal (Cav1.2+/Cav1.3–) strongly reduces wind-up and no PD is observed. *D1* and *E1*, normalized responses plotted against the stimulation number in each condition. *D2* and *E2*, wind-up coefficient.

Mann–Whitney test) (Fig. 7*C1* and *C2*). By contrast, blocking Cav1.3 expression completely suppressed the wind-up of the nociceptive flexion reflex (Fig. 7*A4*) (wind-up coefficient was 510 ± 90, $n = 13$ for Sham and 39 ± 13, $n = 7$ for anti-Cav1.3, $P = 0.0004$, Mann–Whitney test) (Fig. 7*D1* and *D2*). These results confirm *in vivo* the prominent role of Cav1.3 in wind-up in spinal cord circuits.

Decrease of Cav1.3 expression is coupled to a decrease in wind-up amplitude in SNL rats

Under neuropathic conditions, DHNs become hyper-excitable (Chapman *et al.* 1998; Chu *et al.* 2004; Fossat *et al.* 2010) and changes in wind-up are considered to be an indicator of excitability states (Sandkuhler, 2009). Thus, we focused on wind-up amplitude in the SNL model of neuropathy. We first confirmed the neuropathic state by measuring the mechanical threshold of the limb withdrawal reflex in response to mechanical stimulation of the paw to confirm the SNL-induced mechanical allodynia. One week after the surgical procedure, SNL rats presented a strong mechanical allodynia, as reflected by the decrease of the mechanical threshold [from 74 ± 5 g in control (day 0) to 30 ± 1.5 g in SNL (day 7), $n = 14$ rats, $P < 0.0001$, paired t test]. We then analysed the response of DHNs with *in vivo* extracellular recordings in 2–3-month-old rats. We focused on WDR neurons responding to both low and high intensity electrical stimulation. Unexpectedly, wind-up amplitude

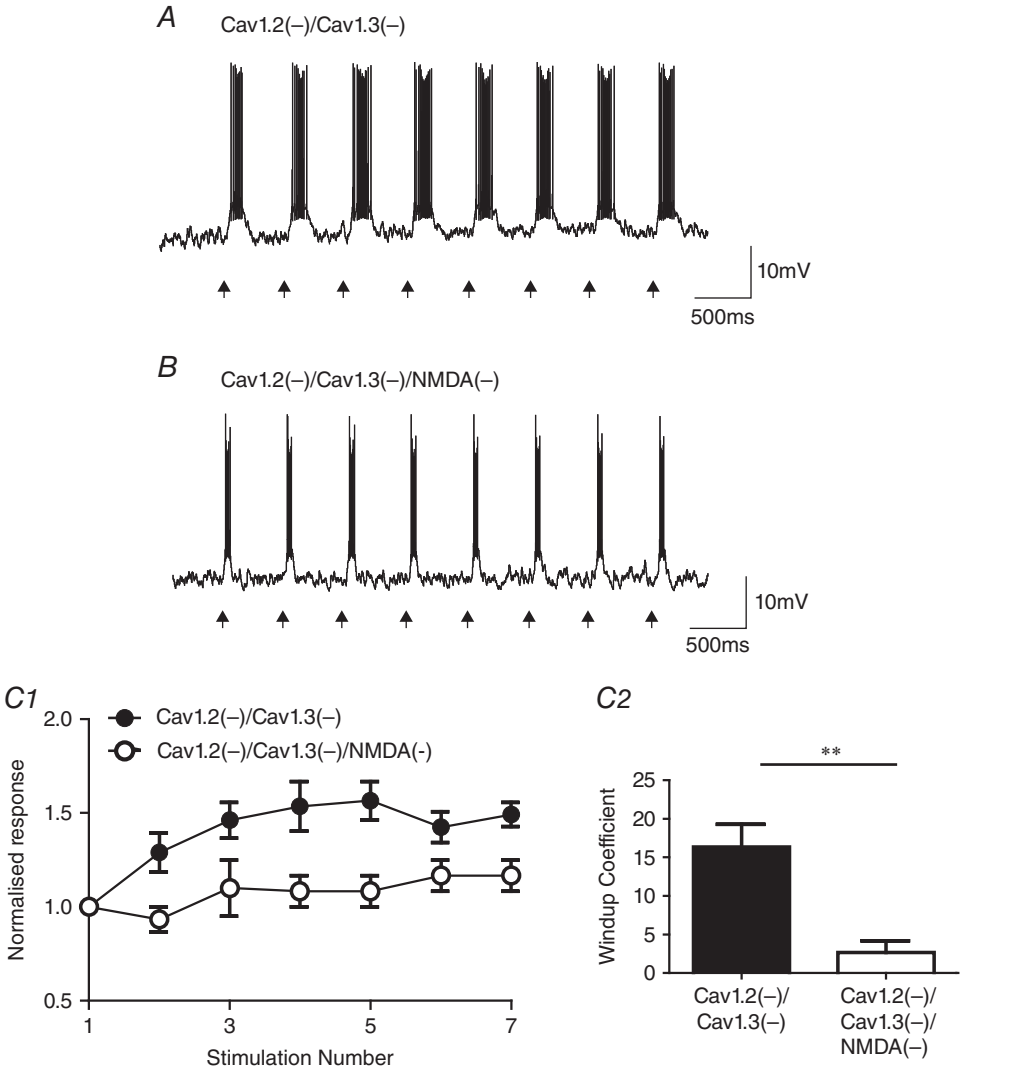

Figure 4. Wind-up also has a synaptic component
A, response of the simulated DHN to repetitive stimulation of C-fibres when Cav1.2 and Cav1.3 are absent. *B*, same protocol but NMDA receptors are also removed. *C1*, normalized response showing that NMDA receptors mediate a slight wind-up (filled circle) that is completely suppressed when NMDA receptors are suppressed (open circles). *C2*, wind-up coefficient.

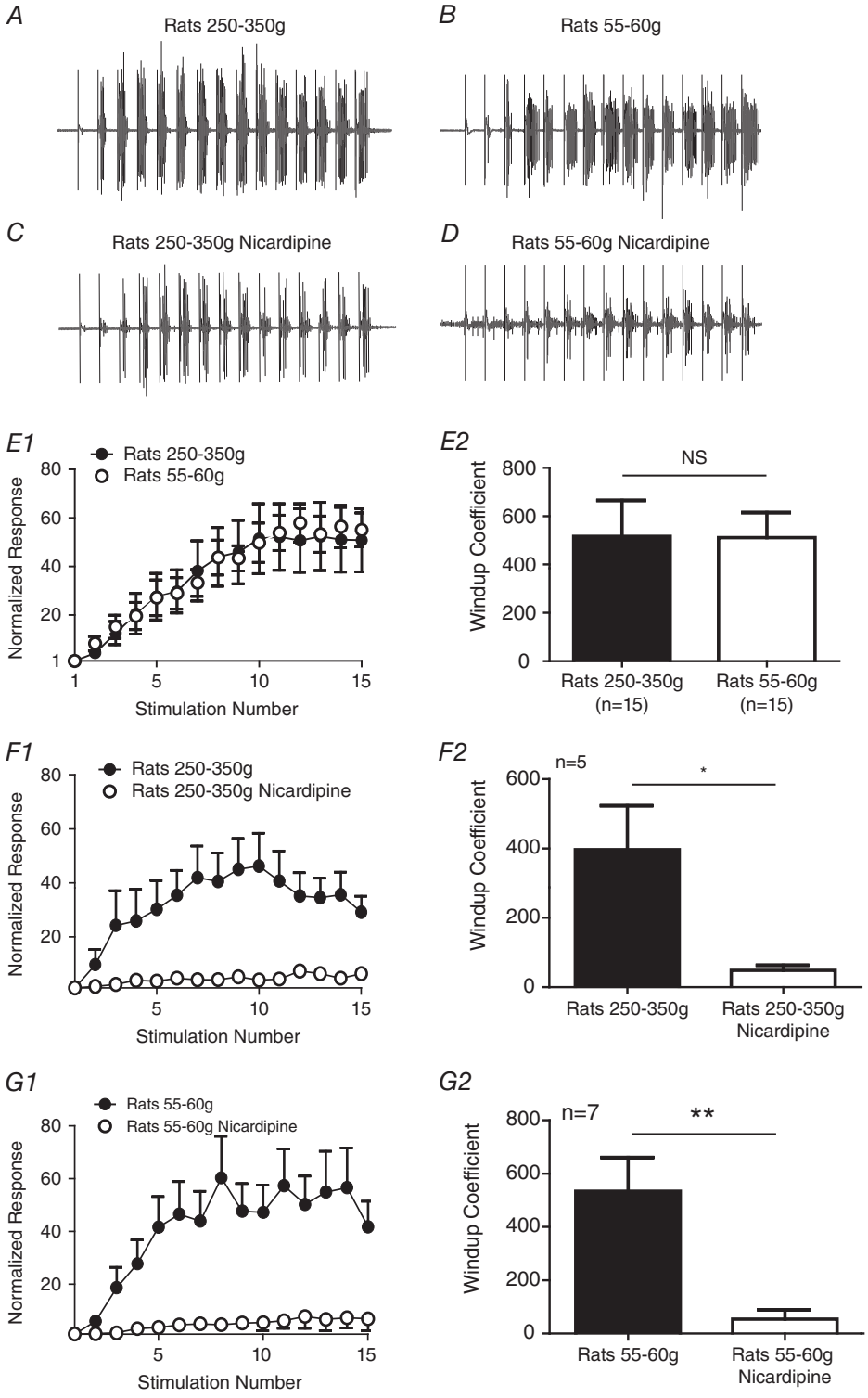

Figure 5. The onset of wind-up depends on LTCs in both young and adult rats
A–D, EMG recordings of the biceps femoris response to electrical stimulation of the ipsilateral paw in the region of the sural nerve. *A* and *C*, in adult rats, before and after intrathecal injection of nicardipine. *B* and *D*, in young rats, before and after intrathecal injection of nicardipine. *E1*, normalized responses plotted against the stimulation number in young and adult rats. *E2*, wind-up coefficient in adult and young rats. *F1*, normalized responses plotted against the stimulation number in adult rats before and after injection of Nicardipine. *F2*, wind-up coefficient. *G1*, normalized responses plotted against the stimulation number in young rats before and after injection of nicardipine. *G2*, wind-up coefficient.

of WDR neurons in SNL rats was significantly decreased compared to naive rats, whereas wind-up amplitude was not modified in sham rats (Fig. 8*A1* and *A2*) [wind-up coefficient was 66 ± 14 (n = 41 DHNs) for SNL rats, 118 ± 4 (n = 119 DHNs) for naive rats and 112 ± 16.5 (n = 6 DHNs) for shams; $P < 0.01$ for SNL *vs.* Naive, Dunn's multiple comparison test). To determine whether a modification of LTC expression could explain this result after the SNL procedure, we performed quantitative RT-PCR to determine changes in LTCs mRNA expression and observed an increase in Cav1.2 mRNA and a decrease in Cav1.3 mRNA (Fig. 8*B*) (Cav1.2 expression in SNL rats was 215 ± 22.9 % of sham expression, $P < 0.01$, Mann–Whitney test; Cav1.3 expression in SNL rats was 60 ± 4.6% of sham expression, $P < 0.05$, Mann–Whitney test). We also measured the immunofluorescence intensity and confirmed the decrease in Cav1.3 and the increase of Cav1.2 expression (Fig. 8*C1–3*) (56.2 ± 11.6% of Sham for Cav1.3; 132 ± 7.3% of Sham for Cav1.2, $P < 0.01$, Mann–Whitney test). However, no change in spatial distribution of Cav1.2 or Cav1.3 was observed after the SNL procedure (Fig. 1*A*).

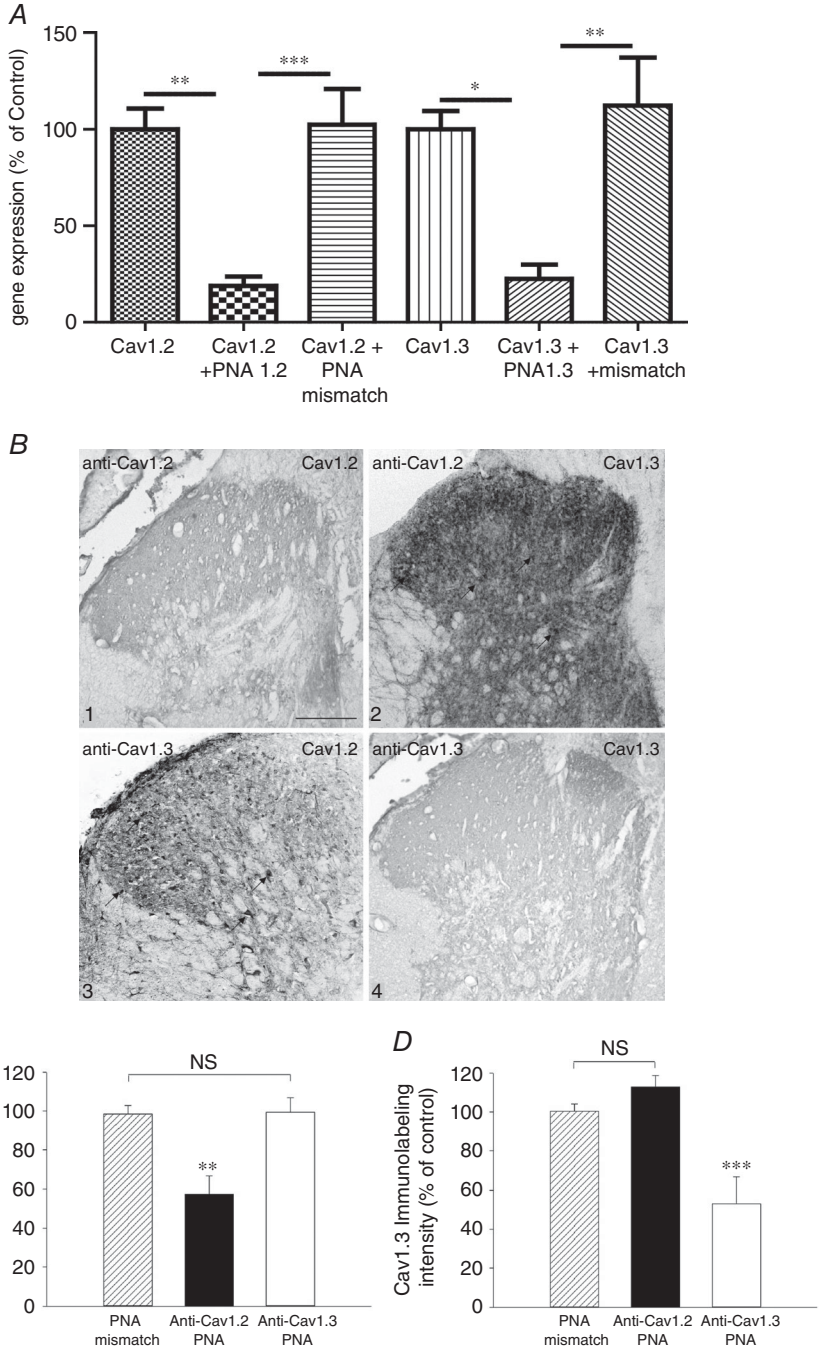

Figure 6. In *vivo* knockdown of Cav subunits
A, quantitative RT PCR of Cav1.2 and Cav1.3 expression following injection of anti-sense PNA molecules. PNA injection elicits a specific blockade upon the anti-sense injected. *B–D*, Cav1.2 and Cav1.3 immunostaining after intrathecal injection of anti-sense molecules targeting Cav1.2 or Cav1.3 mRNA. Note that Cav1.2 labelling is largely decreased after injection of anti-Cav1.2 PNA, whereas Cav1.3 labelling is not affected (*B1*, *B2* and *C*). Reciprocally, Cav1.3 labelling is decreased after injection of AntiCav1.3 PNA, whereas Cav1.2 remained unmodified (*B3*, *B4* and *D*). In (*B*), arrows indicate cell bodies in the dorsal horn of the spinal cord.

Because Cav1.3 is involved in the onset of wind-up in naive rats, we propose that the decrease expression of Cav1.3 in SNL is responsible for the decrease wind-up amplitude in SNL rats. To test this hypothesis, we used the mathematical DHN model to modify LTCs in a fashion similar to the changes observed in mRNA after the SNL procedure (Fig. 8*D*). Repetitive C-fibre stimulations in the model induced a wind-up of DHNs, although the amplitude of the wind-up was clearly decreased (Fig. 8*D1* and *D2*) (the wind-up coefficient was 104 ± 3 in the Naive/sham LTC proportion and 50 ± 4 in the SNL LTC proportion, $n = 6$, $P < 0.01$, Mann–Whitney test). These results indicate that wind-up amplitude is decreased in SNL model of neuropathy and this effect can be reproduced by decreasing Cav1.3 conductances. To confirm the prominent role of the decrease of Cav1.3 expression with respect to the decrease in wind-up amplitude, we used the anti-sense strategy to determine whether the wind-up in SNL is still dependent on Cav1.3 channels. As demonstrated previously (Fossat *et al.* 2010), we first confirmed that SNL-induced mechanical allodynia can be abolished by Cav1.2 expression blockade but not Cav1.3 (Fig. 9) (day 11 after AntiCav1.2, 71 ± 4.1 g, $P = 0.057$ *vs.* day 0; day 11 after Anti-Cav1.3, 29 ± 1.7 g, $P < 0.01$ *vs.* day 0, paired *t* test). We then assessed the consequences of LTC blockade in the onset of wind-up. Cav1.3 expression blockade significantly decreased the amplitude of wind-up, whereas Cav1.2 expression blockade or mismatch had no significant effect on wind-up amplitude (Fig. 10) (wind-up coefficient was 66 ± 14, $n = 41$ for SNL, 26 ± 10, $n = 19$ for SNL + anti-Cav1.3, 47 ± 13, $n = 20$ for SNL + anti-Cav1.2 and 66 ± 26, $n = 10$ for SNL + mismatch, $P = 0.045$ for SNL *vs.* SNL + anti-Cav1.3, p = 0.40 for SNL *vs.* SNL + anti-Cav1.2 and $P = 0.9$ for SNL *vs.* SNL + mismatch, Mann–Whitney test). Altogether, these results suggest that Cav1.3 is the main channel involved in the onset of wind-up, regardless of the physio-pathological conditions, whereas Cav1.2 is involved in SNL-induced DHN hyperexcitability.

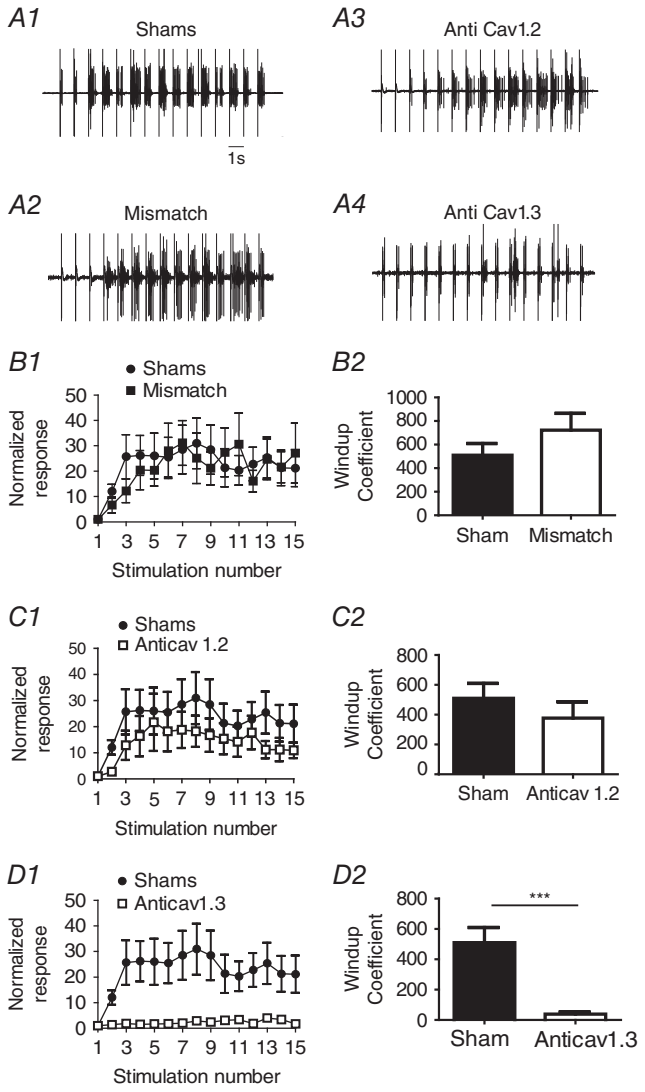

Figure 7. Cav1.3 is responsible for the onset of the wind-up of a nociceptive flexion reflex
A1–A4, EMG recordings of the nociceptive flexion reflex in shams, mismatch-, anti-Cav1.2- or anti-Cav1.3-injected rats (55–60 g). *B1*, normalized responses plotted against the stimulation number in shams and mismatch. *B2*, wind-up coefficient. *C1*, normalized responses plotted against the stimulation number in shams and Anti-Cav1.2 PNA injection. *C2*, wind-up coefficient. *D1*, normalized responses plotted against the stimulation number in shams and Anti-Cav1.3 PNA. *D2*, wind-up coefficient.

Role of plateau and wind-up in neuropathic pain

The decrease in wind-up amplitude after the SNL procedure is surprising because it has already been shown that plateau potentials are more frequent in SNL rats (Reali *et al.* 2011). Thus, we compared the evolution of plateau potentials and wind-up with our mathematical approach under conditions of decreased Cav1.3 expression. We first assessed the consequences of changes in Cav1.3 and Cav1.2 expression in plateau potentials. As shown in Fig. 11*A*, plateau potentials are still expressed in neurones with a decreased expression of Cav1.3 and an increased expression of Cav1.2 (Fig. 11*A1*, naive LTC proportion; Fig. 11*A2*, SNL LTC proportion). Moreover, the amplitude of plateau depends on the stimulation intensity and the maximum amplitude is reached with a lower stimulation intensity in the SNL LTC proportion than in the naive LTC proportion (Fig. 11*A3*). By contrast, the amplitude of wind-up, induced by repetitive short square current pulses, is significantly reduced in the SNL LTC proportion (Fig. 11*B*). These results show that wind-up and plateau potentials are not equivalent in chronic pain conditions. Moreover, plateau expression

is more robust than wind-up. These results suggest that plateaus are not only involved in short-term sensitization in SNL rats, but also in long-term sensitization, where they support prolonged calcium influx.

Discussion

In the present study, we demonstrated that short- and long-term sensitization to pain are controlled by distinct molecular mechanisms. More specifically, our results

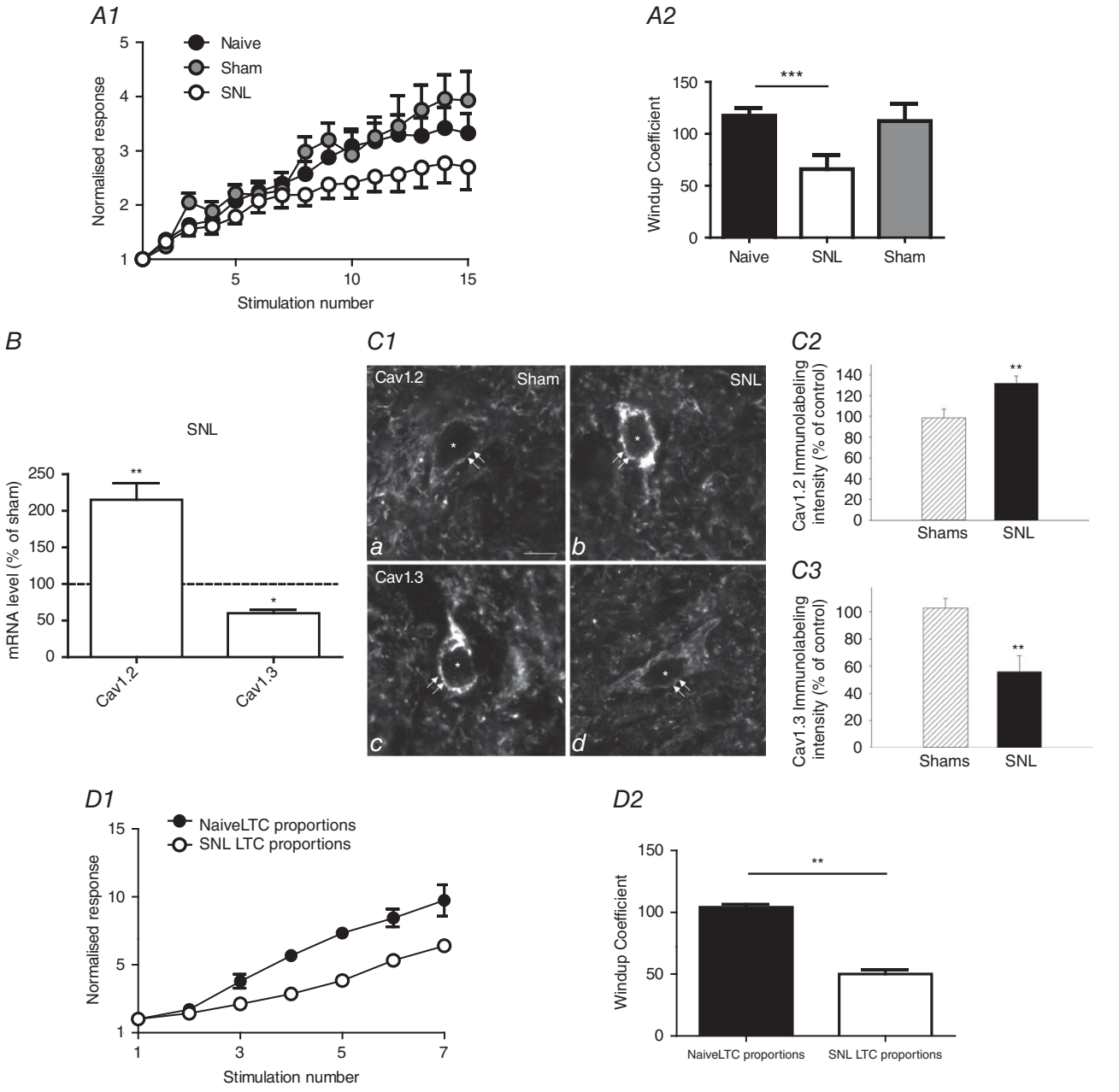

Figure 8. Decrease in Cav1.3 expression and wind-up amplitude in SNL rats
A1, normalized responses of WDR neurons plotted against the stimulation number in naive (black dots, sham (grey dots) and SNL rats (white dots). *A2*, wind-up coefficient. *B*, quantitative RT-PCR reveals a two-fold increase of Cav1.2 expression and a decrease by ~40% of Cav1.3 expression. *C1*, regulation of Cav1.2 (*a* and *b*) and Cav1.3 (*c* and *d*) expression in deep dorsal horn neurons (white stars). *C2*, Cav 1.2 staining is regulated in more intense in neuropathic conditions (SNL, double arrows in C1b) than in control rats (Sham, double arrows in C1a). *C3*, conversely, Cav1.3 labelling is weaker after nerve injury (SNL, double arrows in C1d) than in control rats (Sham, double arrows in C1c). Scale bar = 10 μm. *D1*, normalized responses of modelized DHN plotted against the stimulation number in naive LTCs proportion (black dots) and in SNL LTCs proportions (white dots). *D2*, wind-up coefficient.

indicate a differential role of Cav1.2 and Cav1.3 in DHN excitability. Cav1.3 controls the onset of wind-up in the absence of synaptic influences and significantly increases the amplitude of wind-up when NMDA receptors are present. By contrast, Cav1.2, which have a role on DHN hyper excitability mediated by gene activation under pathological conditions, had no effect on wind-up. Moreover, in a model of neuropathy, we demonstrated that wind-up amplitude is decreased in accordance with a decrease in Cav1.3 mRNA expression. Together, these results reveal that mechanisms for short- and long-term sensitization are distinct phenomena, and that L-type calcium channel subunits independently regulate nociceptive pathway in the short- and long-term sensitization to pain.

VGCCs in pain pathway

VGCCs are a wide family of calcium channels that allow Ca^{2+} influx into the cell. In the central and peripheral nervous system, the high neuronal compartmentalization between the cell body, axons and dendrites gives different cell functions to VGCCs depending on their sub-cellular distribution. Calcium influx through VGCCs is responsible for transmitter release, an increase in neuronal excitability and gene expression. In nociceptive pathways, VGCCs are mainly expressed in the Aδ and C nociceptive fibres and participate in pain transmission. Interestingly, the Cav2.2 subunit constitutes an important calcium influx in Aδ and C nociceptive fibres (Gribkoff, 2006). Moreover, μ opioid receptor-induced inhibition of Cav2.2 sustains opioid-induced analgesia (Seward *et al.* 1991; Bourinet *et al.* 1996). The Cav3.2 subunit is also of major importance in the presynaptic control of pain. Indeed, knockdown of Cav3.2 in nociceptive fibres decreases pain sensitivity in a model of neuropathic pain (Bourinet *et al.* 2005). By contrast, although LTCs do not participate in the acute nociceptive transmission (Diaz and Dickenson, 1997; Fossat *et al.* 2007), they have a role at post-synaptic sites and control excitability and the intrinsic properties of DHNs (Morisset and Nagy, 1999; Heinke *et al.* 2004; Fossat *et al.* 2007). Moreover, LTCs control plateau potentials, a mechanism of input/output amplification that underlies the onset of wind-up in DHNs. In the present study, we show that Cav1.3 is the main conductance responsible for the expression of plateau and wind-up of DHNs. Cav1.2 is also expressed in DHNs but has a minor role in the onset of wind-up; it would rather participate in calcium influx regulating gene expression and mediating long-term changes in DHN excitability associated with neuropathic pain. Indeed, we have confirmed that Cav1.2 expression blockade suppresses the mechanical allodynia and DHN hyperexcitability induced by spinal nerve ligation (Fossat *et al.* 2010). Taken together, these results suggest that the post-synaptic LTCs participate in the large role of VGCCs with respect to amplifying nociceptive responses. Moreover, Cav1.2 is involved in long-term changes, whereas Cav1.3 participates in short-term central sensitization to pain.

Synaptic *vs.* cellular component of wind-up

Wind-up is a form of activity-dependent plasticity of spinal circuits participating in pain processing. In the

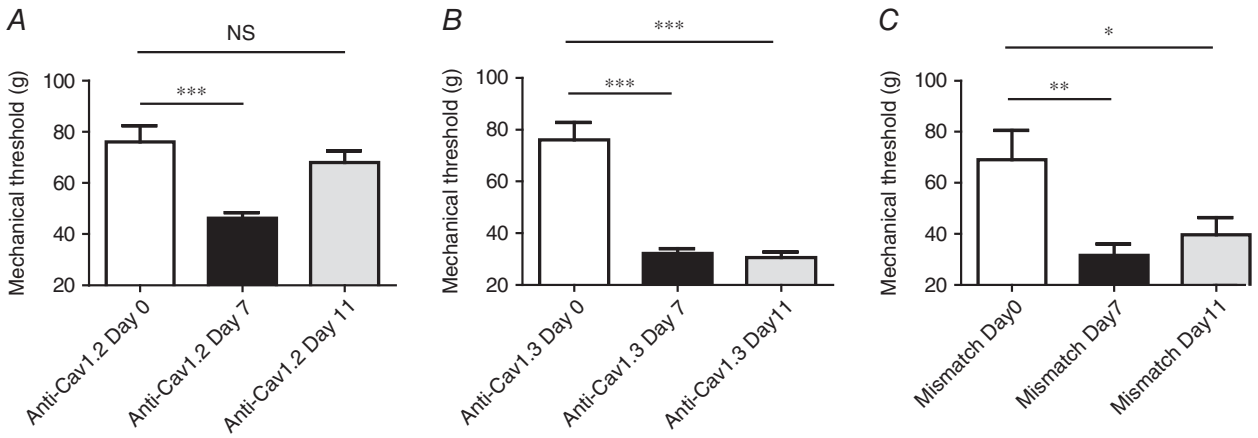

Figure 9. SNL-induced mechanical allodynia is supressed following Anti-Cav1.2 injection
A, SNL procedure (see Methods) induced a significant decrease in the mechanical threshold response 7 days after the nerve ligation (day 7, $P < 0.001$ *vs.* day 0), Repeated-measures ANOVA followed by Bonferroni's multiple comparison test.). SNL-induced allodynia is suppressed by repetitive injection of Anti-Cav1.2 PNA (day 11, $P < 0.05$ *vs.* day 0, repeated-measures ANOVA followed by Bonferroni's multiple comparison test). *B*, injection of Anti-Cav1.3 PNA has no effect on SNL-induced allodynia that persist after repetitive injections at day 11 (day 11, $P < 0.001$ *vs.* day 0, repeated-measures ANOVA followed by Bonferroni's multiple comparison test) *C*, injection of mismatch PNA does not modify the SNL-induced allodynia (day 11, $P < 0.05$ *vs.* day 0, repeated-measures ANOVA followed by Bonferroni's multiple comparison test).

present study, we show that wind-up is mainly controlled by the Cav1.3 subunit of LTCs but not by the Cav1.2 subunit. Thus, Cav1.3 provides DHNs with an intrinsic mechanism for input/output amplification, allowing for prolonged and intense after discharges in response to a brief stimulus. However, wind-up also relies on synaptic plasticity involving NMDA and NK1 receptors (Baranauskas and Nistri, 1998; Herrero *et al.* 2000). Consistently, the results obtained in the present study with our mathematical model, together with previous results, reveal that an excitatory synaptic component such as NMDA or NK1 is also required in a physiological context to trigger wind-up in DHNs (Thompson *et al.* 1990; Fossat *et al.* 2007; Aguiar *et al.* 2010). Moreover, nociceptive fibre activation elicits a complex barrage of excitatory and inhibitory post-synaptic currents in DHNs (Moore *et al.* 2000). Thus, DHNs are influenced by this dynamic balance between the excitatory and inhibitory synaptic inputs where inhibition should be dominated by excitations to trigger plateau potentials and wind-up in

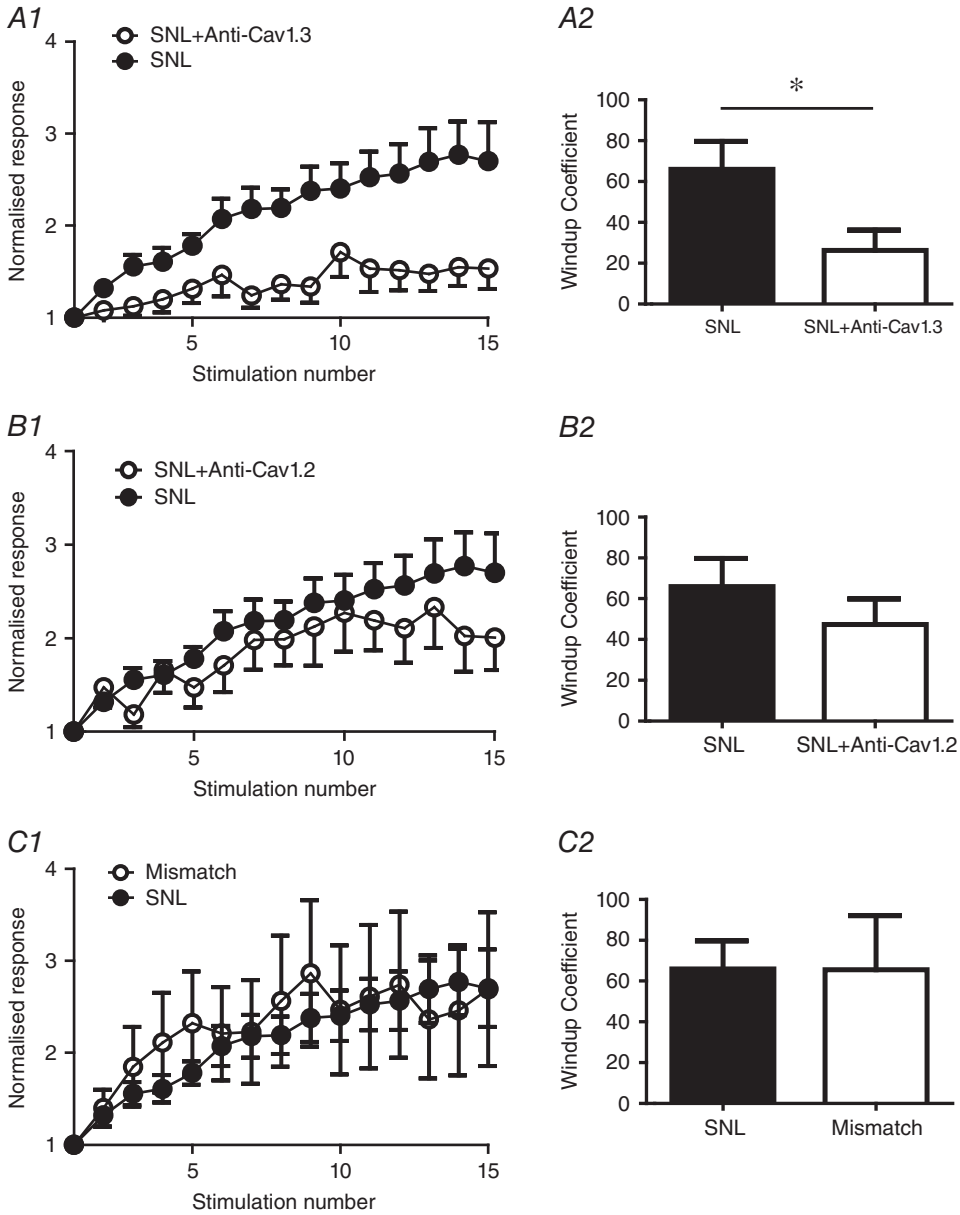

Figure 10. In SNL rats, the onset of wind-up also depends on Cav1.3
A1, normalized responses of WDR neurons plotted against the stimulation number in SNL rats and in SNL rats injected with anti-Cav1.3 PNA. *A2*, wind-up coefficient. *B1*, normalized responses of WDR neurons plotted against the stimulation number in SNL rats and in SNL rats injected with anti-Cav1.2 PNA. *B2*, wind-up coefficient. *C1*, normalized responses of WDR neurons plotted against the stimulation number in SNL rats and in SNL rats injected with mismatch PNA. *C2*, wind-up coefficient.

DHNs following primary afferent stimulation (Fossat *et al.* 2007). Finally, we cannot exclude the possibility that other VGCCs could participate in the onset of wind-up in DHNs. Indeed, a specific Cav3 subunit blocker, ethosuximide, is also able to significantly decrease the amplitude of wind-up in DHNs *in vivo* (Matthews and Dickenson, 2001). However, ethosuximide also decreases the acute nociceptive response, suggesting a presynaptic role of Cav3 channels that would decrease the excitatory synaptic inputs necessary for the onset of wind-up.

Plateau potentials and wind-up in neuropathic pain

Plateau potentials and plateau-dependent wind-up are intrinsic mechanisms for input/output amplification that increase the gain in pain under normal conditions (Morisset and Nagy, 1998; Derjean *et al.* 2003). In other words, they reveal the capacity of DHNs to modify their response to sustained nociceptive inputs (Baranauskas and Nistri, 1998; Li *et al.* 1999) and thus underline a mechanism for protecting a healing zone in the damaged area (Sandkuhler, 2009). Wind-up is also used to characterize central sensitization in pain patients (Staud *et al.* 2007). In fibromyalgia, the amplitude of the temporal summation of the delayed response (i.e wind-up measurement in humans) is increased, which causes an improvement of input/output amplification leading to an amplified pain sensation (Price and Staud, 2005). However, the origin of fibromyalgia is difficult to determine and is not always related to neuropathic pain. Moreover, wind-up and long-term central sensitization as a consequence of nerve lesion are not equivalent (Woolf, 1996). In line with these findings, in the present study, we demonstrate that wind-up amplitude is decreased in the SNL model of neuropathy, whereas plateau amplification remains unaffected. The latter result is in line with previous results showing an increased proportion of plateau expressing neurons under neuropathic conditions (Reali *et al.* 2011). This apparent discrepancy is intriguing because both phenomena share the same molecular partners. Indeed, LTCs are responsible for the active depolarization occurring during a plateau

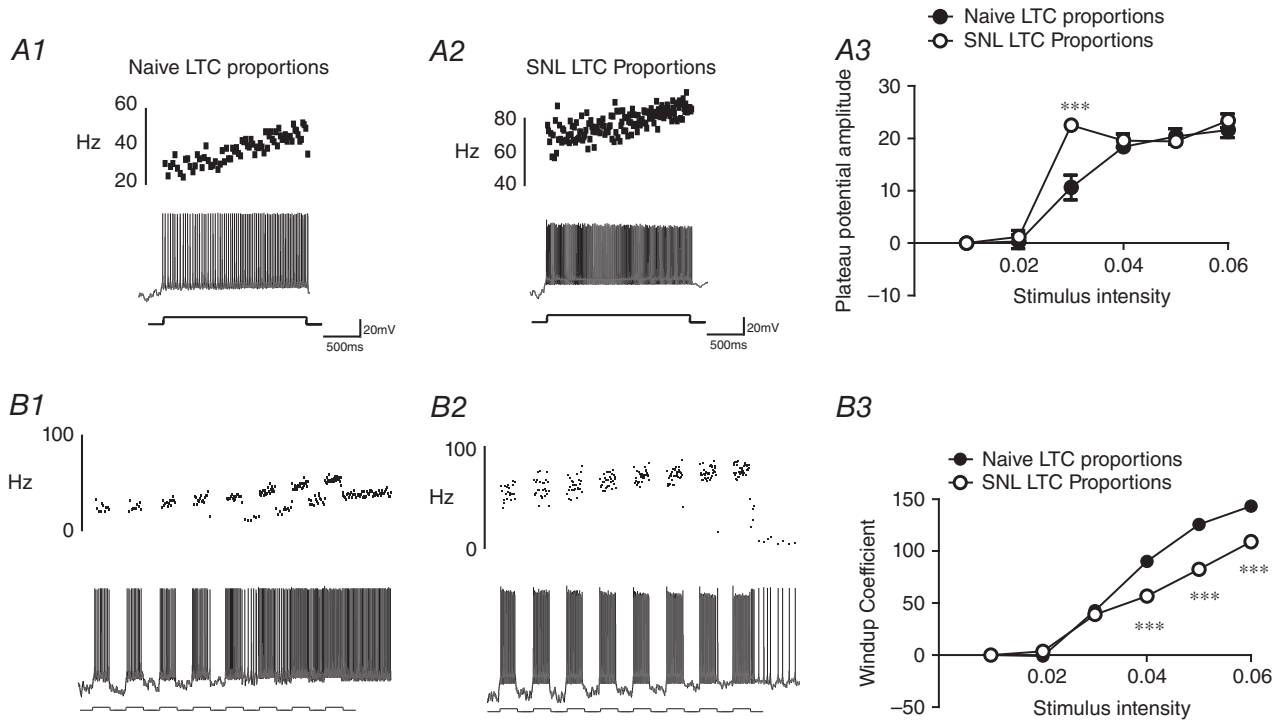

Figure 11. The mathematical approach suggest that plateau potentials and wind-up are not equally affected by changes in LTCs expression
A, a large square current pulse (2 s) elicits a plateau potential in the naive LTC proportion (*A1*), as well as in case of decreased Cav1.3 and increased Cav1.2 expression (SNL LTC proportion) (*A2*). Note that neurons were more responsive to the same stimulus intensity but the difference in instantaneous frequency between the beginning of the square pulse and the end of the square pulse remains similar. The amplitude of plateau is not changed. *A3*, in the naive LTC proportion, as well as in SNL-LTC conditions, plateaus are dependent on stimulus intensity. The maximal plateau amplitude is reached for a lower stimulus intensity in the SNL LTC proportion than in naive LTC proportions. *B1*, wind-up elicited by repetitive square current pulses with the naive LTC proportion. *B2*, wind-up elicited by repetitive square current pulses with the SNL LTC proportion. *B3*, wind-up coefficient plotted against the pulse intensity. Note that, with higher pulse intensity, wind-up coefficient is decreased in the SNL LTC proportion.

protocol and sustained after discharge occurring after the plateau protocol is controlled by cationic non-specific calcium-activated channels (ICAN) (Morisset and Nagy, 1999). This after discharge is a major contributor of the wind-up coefficient. In naive rats, calcium influx through Cav1.3 allows the activation of ICAN and thus sustained after discharge. In SNL rats, Cav1.3 activation during a plateau protocol allows an active depolarization and a discharge acceleration but, because Cav1.3 expression is decreased leading to a decrease in calcium influx, ICAN should be less activated. Thus, plateau amplification is still expressed, whereas the wind-up coefficient is decreased. This discrepancy between wind-up and plateau reveals that both phenomena are not equivalent. Taken together, these results suggest that, in SNL rats, the physiological role of wind-up is decreased. Consequently, the ability to trigger reversible central sensitization as a physiological, protective mechanism is impaired in chronic pain conditions.

LTCs and long-term changes associated with neuropathic pain

Based on their different kinetics and spatial distribution, our mathematical model suggests that Cav1.3 is the intrinsic conductance responsible for the onset of plateau and wind-up. This is further suggested by the anti-sense approach combined with *in vivo* EMG recordings. As already proposed above, the dendritic expression of Cav1.3 coupled to its low activation threshold may allow an active depolarization of the DHN that can be prolonged by other conductances such as ICAN (Morisset and Nagy, 1999; Fossat *et al.* 2007). By contrast, the somatic localization of Cav1.2 and its relative high activation threshold probably makes it unavailable for fast electrical functions. Beside their capacity to modulate membrane potential, LTCs are also involved in long-term changes that mediate cellular mechanisms such as post-synaptic changes and gene expression regulation (Grover and Teyler, 1990; Morgan and Teyler, 1999; Fossat *et al.* 2010; Ma *et al.* 2013; Naka *et al.* 2013). Indeed, in the SNL model of neuropathy, Cav1.2 subunits are known to mediate DHN hyperexcitability through CREB activation and subsequent alteration of gene expression (Fossat *et al.* 2010). These results clearly establish a differential role of LTCs in short- and long-term plasticity in the dorsal horn of the spinal cord. Therefore, modulation of LTCs subunits would be a crucial phenomenon for both the capacity of DHNs to integrate afferent inputs (i.e role of Cav1.3) and DHN hyperexcitability in chronic pain states (i.e role of Cav1.2).

In conclusion, we have demonstrated that short- and long-term sensitization to pain in the spinal cord relies on distinct mechanisms with a differential role of LTCs subunits. These results suggest that plateau potentials and wind-up are physiological mechanisms that contribute to an efficient nociceptive transmission but are impaired in neuropathic pain. Finally, therapeutic approaches that target regulators of Cav1.2 -mediated changes in gene expression may be more relevant than those that target plateau potentials and wind-up.

References

Aguiar P, Sousa M & Lima D (2010). NMDA channels together with L-type calcium currents and calcium-activated nonspecific cationic currents are sufficient to generate windup in WDR neurons. *J Neurophysiol* **104**, 1155–1166.

Baranauskas G & Nistri A (1998). Sensitization of pain pathways in the spinal cord: cellular mechanisms. *Prog Neurobiol* **54**, 349–365.

Basbaum AI, Bautista DM, Scherrer G & Julius D (2009). Cellular and molecular mechanisms of pain. *Cell* **139**, 267–284.

Bourinet E, Alloui A, Monteil A, Barrere C, Couette B, Poirot O, Pages A, McRory J, Snutch TP, Eschalier A & Nargeot J (2005). Silencing of the Cav3.2 T-type calcium channel gene in sensory neurons demonstrates its major role in nociception. *EMBO J* **24**, 315–324.

Bourinet E, Soong TW, Stea A & Snutch TP (1996). Determinants of the G protein-dependent opioid modulation of neuronal calcium channels. *Proc Natl Acad Sci USA* **93**, 1486–1491.

Chapman V, Suzuki R & Dickenson AH (1998). Electrophysiological characterization of spinal neuronal response properties in anaesthetized rats after ligation of spinal nerves L5-L6. *J Physiol* **507**, 881–894.

Chu KL, Faltynek CR, Jarvis MF & McGaraughty S (2004). Increased WDR spontaneous activity and receptive field size in rats following a neuropathic or inflammatory injury: implications for mechanical sensitivity. *Neurosci Lett* **372**, 123–126.

Derjean D (2002). Propriétés membranaires et contrôle neuromodulateur inhibiteur des neurones nociceptifs profonds de la moelle épinière: Approche électrophysiologique *in vitro* chez le rat. *PhD Thesis*, University of bordeaux-Segalen, Bordeaux, France.

Derjean D, Bertrand S, Le Masson G, Landry M, Morisset V & Nagy F (2003). Dynamic balance of metabotropic inputs causes dorsal horn neurons to switch functional states. *Nat Neurosci* **6**, 274–281.

Diaz A & Dickenson AH (1997). Blockade of spinal N- and P-type, but not L-type, calcium channels inhibits the excitability of rat dorsal horn neurones produced by subcutaneous formalin inflammation. *Pain* **69**, 93–100.

Dobremez E, Bouali-Benazzouz R, Fossat P, Monteils L, Dulluc J, Nagy F & Landry M (2005). Distribution and regulation of L-type calcium channels in deep dorsal horn neurons after sciatic nerve injury in rats. *Eur J Neurosci* **21**, 3321–3333.

Egholm M, Buchardt O, Christensen L, Behrens C, Freier SM, Driver DA, Berg RH, Kim SK, Norden B & Nielsen PE (1993). PNA hybridizes to complementary oligonucleotides obeying the Watson–Crick hydrogen-bonding rules. *Nature* **365**, 566–568.

Favereaux A, Thoumine O, Bouali-Benazzouz R, Roques V, Papon MA, Salam SA, Drutel G, Leger C, Calas A, Nagy F & Landry M (2011). Bidirectional integrative regulation of Cav1.2 calcium channel by microRNA miR-103: role in pain. *EMBO J* **30**, 3830–3841.

Fossat P, Dobremez E, Bouali-Benazzouz R, Favereaux A, Bertrand SS, Kilk K, Leger C, Cazalets JR, Langel U, Landry M & Nagy F (2010). Knockdown of L calcium channel subtypes: differential effects in neuropathic pain. *J Neurosci* **30**, 1073–1085.

Fossat P, Sibon I, Le Masson G, Landry M & Nagy F (2007). L-type calcium channels and NMDA receptors: a determinant duo for short-term nociceptive plasticity. *Eur J Neurosci* **25**, 127–135.

Gozariu M, Bragard D, Willer JC & Le Bars D (1997). Temporal summation of C-fibre afferent inputs: competition between facilitatory and inhibitory effects on C-fibre reflex in the rat. *J Neurophysiol* **78**, 3165–3179.

Gribkoff VK (2006). The role of voltage-gated calcium channels in pain and nociception. *Semin Cell Dev Biol* **17**, 555–564.

Grover LM & Teyler TJ (1990). Two components of long-term potentiation induced by different patterns of afferent activation. *Nature* **347**, 477–479.

Heinke B, Balzer E & Sandkuhler J (2004). Pre- and postsynaptic contributions of voltage-dependent Ca^{2+} channels to nociceptive transmission in rat spinal lamina I neurons. *Eur J Neurosci* **19**, 103–111.

Helton TD, Xu W & Lipscombe D (2005). Neuronal L-type calcium channels open quickly and are inhibited slowly. *J Neurosci* **25**, 10247–10251.

Herrero JF, Laird JM & Lopez-Garcia JA (2000). Wind-up of spinal cord neurones and pain sensation: much ado about something? *Prog Neurobiol* **61**, 169–203.

Kim SH & Chung JM (1992). An experimental model for peripheral neuropathy produced by segmental spinal nerve ligation in the rat. *Pain* **50**, 355–363.

Koch T, Hansen HF, Andersen P, Larsen T, Batz HG, Otteson K & Orum H (1997). Improvements in automated PNA synthesis using Boc/Z monomers. *J Pept Res* **49**, 80–88.

Lambert RC, McKenna F, Maulet Y, Talley EM, Bayliss DA, Cribbs LL, Lee JH, Perez-Reyes E & Feltz A (1998). Low-voltage-activated Ca^{2+} currents are generated by members of the CavT subunit family (alpha1G/H) in rat primary sensory neurons. *J Neurosci* **18**, 8605–8613.

Li J, Simone DA & Larson AA (1999). Windup leads to characteristics of central sensitization. *Pain* **79**, 75–82.

Livak KJ & Schmittgen TD (2001). Analysis of relative gene expression data using real-time quantitative PCR and the 2(-Delta Delta C(T)) method. *Methods* **25**, 402–408.

Ma H, Cohen S, Li B & Tsien RW (2013). Exploring the dominant role of Cav1 channels in signalling to the nucleus. *Biosci Rep* **33**, 97–101.

Matthews EA & Dickenson AH (2001). Effects of ethosuximide, a T-type Ca(2+) channel blocker, on dorsal horn neuronal responses in rats. *Eur J Pharmacol* **415**, 141–149.

Moore KA, Baba H & Woolf CJ (2000). Synaptic transmission and plasticity in the superficial dorsal horn. *Prog Brain Res* **129**, 63–80.

Morgan SL & Teyler TJ (1999). VDCCs and NMDARs underlie two forms of LTP in CA1 hippocampus in vivo. *J Neurophysiol* **82**, 736–740.

Morisset V & Nagy F (1998). Nociceptive integration in the rat spinal cord: role of non-linear membrane properties of deep dorsal horn neurons. *Eur J Neurosci* **10**, 3642–3652.

Morisset V & Nagy F (1999). Ionic basis for plateau potentials in deep dorsal horn neurons of the rat spinal cord. *J Neurosci* **19**, 7309–7316.

Morisset V & Nagy F (2000). Plateau potential-dependent windup of the response to primary afferent stimuli in rat dorsal horn neurons. *Eur J Neurosci* **12**, 3087–3095.

Naka A, Gruber-Schoffnegger D & Sandkuhler J (2013). Non-Hebbian plasticity at C-fibre synapses in rat spinal cord lamina I neurons. *Pain* **154**, 1333–1342.

Pooga M, Soomets U, Bartfai T & Langel U (2002). Synthesis of cell-penetrating peptide-PNA constructs. *Methods Mol Biol* **208**, 225–236.

Price DD & Staud R (2005). Neurobiology of fibromyalgia syndrome. *J Rheumatol Suppl* **75**, 22–28.

Reali C, Fossat P, Landry M, Russo RE & Nagy F (2011). Intrinsic membrane properties of spinal dorsal horn neurones modulate nociceptive information processing in vivo. *J Physiol* **589**, 2733–2743.

Sandkuhler J (2009). Models and mechanisms of hyperalgesia and allodynia. *Physiol Rev* **89**, 707–758.

Seward E, Hammond C & Henderson G (1991). Mu-opioid-receptor-mediated inhibition of the N-type calcium-channel current. *Proc Biol Sci* **244**, 129–135.

Simon M, Perrier JF & Hounsgaard J (2003). Subcellular distribution of L-type Ca^{2+} channels responsible for plateau potentials in motoneurons from the lumbar spinal cord of the turtle. *Eur J Neurosci* **18**, 258–266.

Soomets U, Lindgren M, Gallet X, Hallbrink M, Elmquist A, Balaspiri L, Zorko M, Pooga M, Brasseur R & Langel U (2000). Deletion analogues of transportan. *Biochim Biophys Acta* **1467**, 165–176.

Staud R, Robinson ME & Price DD (2007). Temporal summation of second pain and its maintenance are useful for characterizing widespread central sensitization of fibromyalgia patients. *J Pain* **8**, 893–901.

Suzuki R, Matthews EA & Dickenson AH (2001). Comparison of the effects of MK-801, ketamine and memantine on responses of spinal dorsal horn neurones in a rat model of mononeuropathy. *Pain* **91**, 101–109.

Thompson SW, King AE & Woolf CJ (1990). Activity-dependent changes in rat ventral horn neurons in vitro; summation of prolonged afferent evoked postsynaptic depolarizations produce a d-2-amino-5-phosphonovaleric acid sensitive windup. *Eur J Neurosci* **2**, 638–649.

Woolf CJ (1991). Generation of acute pain: central mechanisms. *Br Med Bull* **47**, 523–533.

Woolf CJ (1996). Windup and central sensitization are not equivalent. *Pain* **66**, 105–108.

Xu W & Lipscombe D (2001). Neuronal Ca(V)1.3alpha(1) L-type channels activate at relatively hyperpolarized membrane potentials and are incompletely inhibited by dihydropyridines. *J Neurosci* **21**, 5944–5951.

Additional information

Competing interests

The authors declare that they have no competing interests.

Author contribution

HR, MJL-G, DC, ED, RB, AF and PF were responsible for the collection and assembly of data. HR, MJL-G, DC, ED, ML and PF were responsible for data analysis and interpretation. EE and ÜL were responsible for the provision of study materials or patients. AF, ML and PF were responsible for the study conception and design. AF, ME, ML and PF were responsible for writing the manuscript. All authors agree to be accountable for all aspects of the work, ensuring that questions related to the accuracy or integrity of any part are appropriately investigated and resolved. All persons designated as authors qualify for authorship, and all those who qualify for authorship are listed.

Funding

This work was supported by Conseil Général d'Aquitaine (N°11004369/11004370), Agence National pour la Recherche (ANR MirPain), Labex 'BRAIN', IRSES 'Neuren' n°6A-2012-318997, Erasmus Mundus Green It.

Acknowledgements

We thank Bordeaux Imaging Centre (BIC), UMS 3420 CNRS, Université de Bordeaux, US4, INSERM; Professor D. Voisin for careful reading of the manuscript; Professor A. Gundlach for editing the English language prior to submission; and Sébastien Benquet for technical support.